J Biomol NMR (2007) 37:97–111
DOI 10.1007/s10858-006-9109-7

ARTICLE

Separated local field NMR experiments on oriented samples rotating at the magic angle

Jakob J. Lopez · A. J. Mason · Christoph Kaiser · Clemens Glaubitz

Received: 8 August 2006 / Accepted: 13 October 2006 / Published online: 19 December 2006

Abstract Biophysical studies on membrane proteins by solid state NMR (SSNMR) can be carried out directly in a membrane environment. Samples are usually prepared in form of multi-lamellar dispersions for magic angle sample spinning or as aligned multi-layers for orientation dependent NMR experiments without sample rotation. A new development is the application of MAS NMR to aligned samples (MAOSS; Magic Angle Oriented Sample Spinning). In combination with separated local field (SLF) experiments, size and orientation of heteronuclear dipolar couplings may be extracted from two-dimensional experiments which correlate dipolar couplings with isotropic chemical shifts. The orientation of these ^{1}H–X dipolar couplings can be directly related to the orientation of molecular groups in the sample. Here, we demonstrate the feasibility of these experiments on highly ordered polyethylene fibers which serve as model compound. Based on these data, the experiment is also applied to ordered multi-layers of bacteriorhodopsin (purple membrane) which is used as a model for aligned membrane proteins. We present a detailed analysis of different experimental designs with respect to angular sensitivity and the influence of residual sample disorder (''mosaic spread''). The results of the MAOSS-SLF experiment are discussed within the context of established solid state NMR experiments which are usually performed without sample rotation and we compare the data to orientation information obtained from X-ray diffraction.

Keywords Dipolar couplings · Separated local field · Solid state NMR · MAS · Membrane proteins · Ordered samples

J. J. Lopez · C. Kaiser · C. Glaubitz (✉)
Institute for Biophysical Chemistry and Center for Biomolecular Magnetic Resonance, J.W. Goethe University, Max von Laue Str. 9, 60438 Frankfurt am Main, Germany
e-mail: glaubitz@em.uni-frankfurt.de

A. J. Mason
Faculté de Chimie, Université Louis Pasteur/CNRS LC3-UMR7177, Institut le Bel, 4 rue Blaise Pascal, F-67070 Strasbourg, France

Introduction

Solid state nuclear magnetic resonance (SS-NMR) can be used to obtain detailed structural information of membrane proteins and membrane-bound peptides at high resolution by either uniform or selective isotope labeling. Distance constraints and isotropic chemical shift data are available from MAS-NMR (Luca et al. 2003; Rienstra et al. 2000), while the orientation dependence of a nuclear spin interaction is exploited by NMR on macroscopically aligned samples (Opella et al. 2001; Sizun and Bechinger 2002). The interpretation of these constraints is based on the exact knowledge of the spin interaction tensors, including the tensor element magnitudes, and their orientation with respect to the molecular frame (Cross and Quine 2000; Quine and Cross 2000). These orientation constraints have been gathered by static methods, i.e. without sample rotation, through line-shape analyses of one-dimensional spectra (Mai et al. 1993; Ulrich and Watts 1993), or by multi-dimensional experiments such as DECODER (Schmidt-Rohr et al. 1992) and PISEMA (Wu et al. 1994).

Under MAS conditions, orientational data have been obtained from membrane samples aligned on a solid support which has been placed into an MAS rotor (Glaubitz and Watts 1998; Sizun and Bechinger 2002). In these MAOSS (magic angle oriented sample spinning) experiments (Glaubitz and Watts 1998), spinning sideband patterns arising from ^{13}C and ^{15}N chemical shift anisotropies (CSA) (Glaubitz et al. 2000; Mason et al. 2004) and ^{2}H quadrupole couplings, have been used (Glaubitz et al. 1999). Other applications have also seen the use of ^{31}P CSA spinning sideband patterns on ordered DNA fibers (van Dam and Levitt 2000) and ^{13}C CSA data on ordered polymers (Schmidt-Rohr and Spiess 1994).

It is important to note that dipolar couplings (DC) are linked to structural parameters in a more straightforward manner than the CSA, as they point along vectors which connect two coupled nuclei. Consequently, MAOSS SS-NMR experiments with specifically designed dipolar recoupling methods are currently of great interest, and are paving the way for measurements of the size and orientation of internuclear vectors. In a very promising example, three-dimensional orientations of heteronuclear bond vectors have been determined for the case of a single crystalline amino acid by REDOR measurements on oriented samples under MAS conditions (Gross et al. 2005).

Here, we present a simple and straightforward approach to measure nuclear bond orientations in membrane proteins by applying separated local field (SLF) experiments to ordered samples. Instead of using a recoupling experiment, the sample rotation about the magic angle is kept to a modest speed which removes the dipolar coupling only partly, but nevertheless facilitates a spectrum with a well resolved chemical shift resolution. With this method, the ^{1}H–X dipolar couplings for various resolved sites X may be obtained simultaneously within one experiment. In the MAOSS-SLF experiment, the ^{1}H–X dipolar coupling can be obtained directly from the FID in the indirect dimension sampled over one rotor period where the spin system evolves under the sole influence of the ^{1}H–X dipolar coupling. The modulation of these dipolar evolution curves (DEC), depends on size and orientation of the dipolar coupling tensor with respect to the MAS rotor symmetry axis (Fig. 1a). A proton bound to a nucleus X along a vector which is collinear with the axis of the MAS rotor ($\beta_{PR} = 0$), will exhibit a DEC which shows no modulation. The shape of the DECs change with deviations of the internuclear vector from the magic angle ($\beta_{PR} > 0$), and the angular values of the internuclear vectors can be obtained by fitting calculated DECs to the experimental curve as a function of the angle β_{PR}.

In the following, we will demonstrate this experiment on ordered polyethylene (PE) as well as on aligned multi-layers of bacteriorhodopsin (BR). PE is a structurally simple polymer of the form CH_3–$(CH_2)_n$–CH_3, which has been investigated extensively by solid state

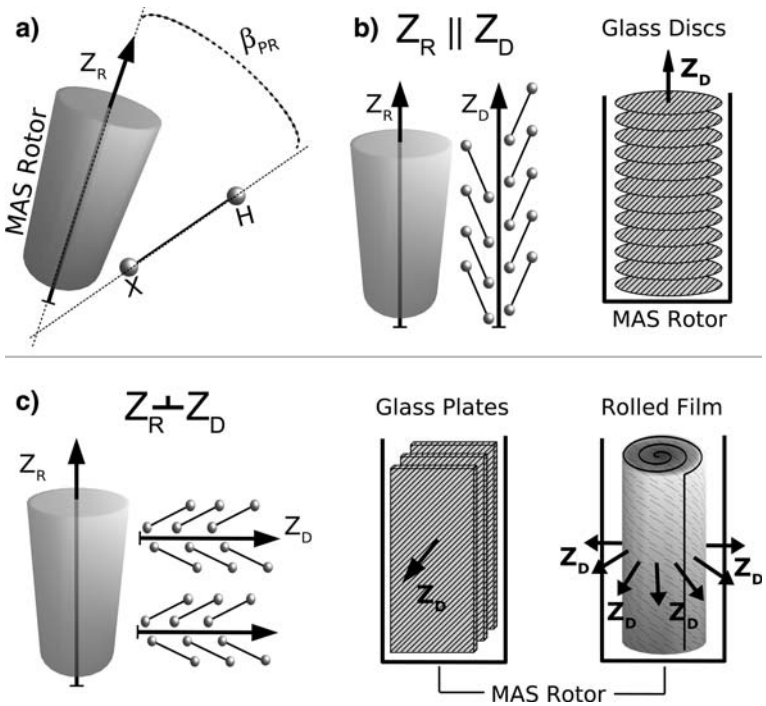

Fig. 1 The angle β_{PR} is spanned by the internuclear vector between nucleus X and H and the MAS rotor axis (**a**). Glass plates with aligned membrane samples can be placed with the sample director parallel (**b**) or perpendicular (**c**) to the MAS rotor axis (Glaubitz and Watts 1998). Sample alignments on polymer films rolled up (**c**) and inserted into an MAS rotor have been demonstrated as well (Sizun and Bechinger 2002)

NMR (Fischbach et al. 2004; Opella and Waugh 1977). BR is the light-driven proton pump of *H. Salinarium*. It is a 26 kDa membrane protein with a seven transmembrane α-helix topology. BR forms a two-dimensional hexagonal crystalline lattice which is arranged in trimeric units in the native purple membrane. Purple membrane orients well on glass plates, which preserves the directional character of the protein, and maintains structural and functional integrity under a wide range of conditions. BR has been extensively studied with a large range of methods and therefore makes an excellent model system (Lanyi 2004).

For orientation dependent experiments, membrane samples are usually aligned on a solid support such as polymer films or glass plates. Depending on the experiments, the sample director Z_D can take different orientations with respect to the applied magnetic field. For MAS-NMR on aligned samples, three different experimental designs have been suggested: Glass plates can either be placed in the MAS rotor with the membrane normal parallel ($Z_D \| Z_R$) or perpendicular ($Z_D \perp Z_R$) to the MAS rotor axis as illustrated in Fig. 1b and 1c (Glaubitz and Watts 1998). Furthermore, the alignment on polymer films which take a cylindrical distribution with $Z_D \perp Z_R$ in the MAS rotor has been demonstrated to be especially useful for smaller MAS rotors and higher spinning speeds as the centrifugal forces caused by sample rotation support sample alignment (Fig. 1 c) (Sizun and Bechinger 2002). Without rotor-synchronized data acquisition, both cases in Fig. 1c show an effective carousel symmetry around Z_R.

Although the angle β_{PR} describes the tilt of the dipolar coupling with respect to the MAS rotor axis, a number of coordinate transformations are needed in order to link this angle to molecular parameters. The hierarchy of reference frames for PE fibers is illustrated in Fig.2a and for aligned multi-layers of bacteriorhodopsin in Fig. 2b. A set of Euler angles Ω_{PD} is needed to rotate the dipolar coupling tensor into the

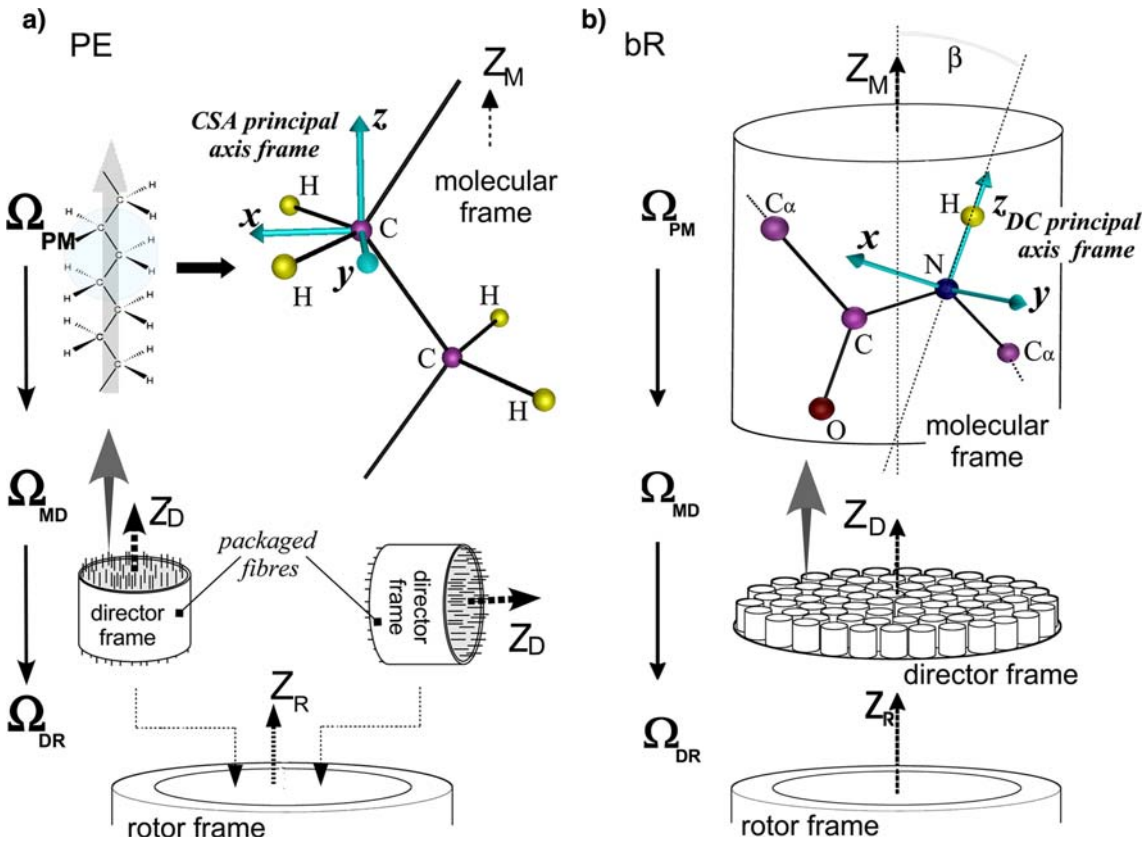

Fig. 2 The hierarchy of reference frames for the NMR interactions considered here is illustrated for PE (**a**) and BR (**b**). A set of Euler angles Ω_{PM} is needed to rotate the principal axis system P into the molecular frame M which is related to the sample director frame D by Ω_{MD}. This is again transferred into the MAS rotor frame R by Ω_{DR}. For the case of PE, the molecular reference frame M is defined by the fiber long axis Z_M which is also the main axis of molecular order and therefore defines the sample director Z_D as well. The orientation of the C–H dipolar coupling is measured with respect to Z_M or Z_D. In case of BR, Z_D is the membrane normal to which the dipolar N–H coupling is tilted by β. In both systems, molecules follow a two-dimensional distribution around Z_D. In addition, sample disorder is characterized by a misalignment of Z_D (mosaic spread, see text)

sample director frame D which is defined by the main axis of molecular order. In case of PE, this is the fiber long axis and in case of membrane samples the membrane normal. Here, we are interested in the orientation of the dipolar coupling with respect to the sample director frame D which is described by the tilt angle β_{PD}. For the sake of simplicity, we will omit indices and refer to this angle as β in the rest of this work.

As we deal with partially ordered and not single crystal samples, the orientation distribution of the molecules in the sample director frame with respect to the MAS rotor frame has to be considered. Both samples in Fig. 2 show carousel symmetry around Z_D. In addition, sample disorder is approximated by a distribution of the orientation of Z_D around Z_R with a Gaussian form, as assumed also in other works (Nevzorov et al. 1999; Quine and Cross 2000). In other studies, the source of the error in protein alignment has been attributed mainly to hydration levels and solvent effects (Moll and Cross 1990; Nicholson et al. 1987).

The experimental situation discussed here is illustrated in Fig. 3. For a full powder distribution, Z_D can take every orientation and a spectrum is calculated by summing up spectra for each individual orientation multiplied with a weighing factor which is illustrated by the length of each rod in Fig. 3a. The orientation distribution of Z_D in the sample arrangement shown in Fig. 1b ($Z_D \| Z_R$) and 1c ($Z_D \perp Z_R$) is illustrated in Fig. 3b and c, respectively. The sample director Z_D is assumed to adhere to a Gaussian distribution (Nevzorov et al. 1999; Quine and Cross 2000) with a width of $\Delta\beta$ (mosaic spread). Samples with $Z_D \perp Z_R$ and additional carousel symmetry around Z_R such as membranes aligned on rolled up polymer films (Fig. 1c) cover a larger range of Euler angles (Fig. 3d). A similar distribution can be assumed for ordered PE fibers (Fig. 2a). Full simulation details are explained and discussed further below.

To test experiment and simulation software on a model system, we used ordered polyethylene, with the main axis of molecular order parallel and perpendicular to the MAS rotor axis (Fig. 2a).

In order to choose the best of all suggested sample geometries (Fig. 1b and c) for experiments on bacteriorhodopsin, we have examined the influence of the sample arrangement and the mosaic spread on the expected tilt angle resolution. The comparison was carried out by numerically simulating SLF experiments for different geometries. The results indicate with which degree of accuracy the tilt angle β can be

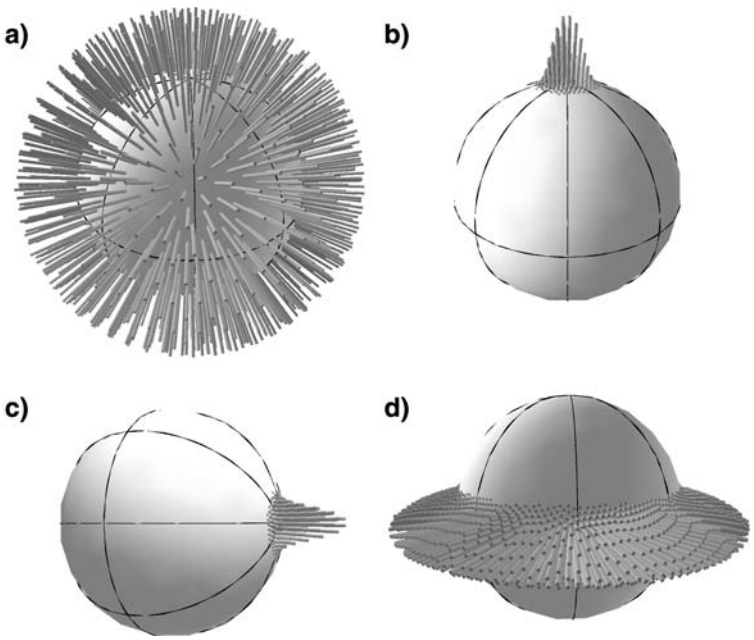

Fig. 3 Graphical representations of the molecular distribution in the partially ordered samples discussed here (Figs. 1 and 2). For the simulation of MAS spectra, the orientational distribution of a molecular ensemble has to be taken into account. In case of powder samples, all molecular orientations are possible and contribute with a weighing factor represented by the length of each rod in (**a**). In ordered samples as PE fibers or BR multi-layers with $Z_D \| Z_R$ (**b**) or $Z_D \perp Z_R$ (**c**) molecular misalignment is described by a Gaussian distribution of the local alignment axis (mosaic spread $\Delta\beta$). In case of samples with $Z_D \perp Z_R$ and additional cylinder symmetry around Z_R as shown in Fig. 1c, a more complex orientational distribution is obtained (**d**). Calculations were carried out using the REPULSION algorithm (Bak and Nielsen 1997) and a mosaic spread of 10° (see text for details)

determined and in which range of angles both approaches are most sensitive.

Building upon these simulations and the experimental results obtained from PE, we applied ^{15}N–^{1}H-SLF experiments to ^{15}N-methionine labeled bacteriorhodopsin (BR) in purple membrane patches aligned on glass plates. We compare the results of these SLF-MAOSS experiments with those of PISEMA experiments which were carried out on similar samples, as reported by Nielsen and Watts (Kamihira et al. 2005). General theoretical and experimental aspects are discussed.

Materials and methods

Separated local field NMR experiments

The SLF experiment was first performed in the mid 1970s (Waugh 1976) and is described abundantly in literature (Hester et al. 1976; Munowitz and Griffin 1982; Munowitz et al. 1981; Ramamoorthy and Opella 1995; Schmidt-Rohr and Spiess 1994; Song et al. 2001). For the sake of brevity, only a brief description is given here. The ^{1}H–X dipolar coupling (PE: X = ^{13}C, BR: X = ^{15}N) is extracted by separating chemical shift and dipolar couplings into two dimensions: Cross polarized X magnetization evolves for a variable time interval t_1 in the presence of phase modulated Lee-Goldburg (PMLG) ^{1}H–^{1}H decoupling (Lee and Goldburg 1965; Vinogradov et al. 1999). PMLG is followed by proton decoupling for an interval τ_R–t_1, where τ_R is the rotor period. A 180° X pulse is applied and protons are decoupled for another period of τ_R. The total time interval is kept constant to $2\tau_R$ to eliminate modulations due to the chemical shift anisotropy of nuclei X.

Fourier transformation is carried out in ω_2 only. The intensity modulation during t_1 over one full rotor period describes a dipolar evolution curve (DEC) for each resolved site X.

All experiments were carried out on a Bruker Avance spectrometer with a 7 mm DVT probehead at ν_0 = –400.13 MHz for ^{1}H, –100.6 MHz for ^{13}C and 40.54 MHz for ^{15}N.

PMLG decoupling was set up on adamantane by varying the ^{1}H r.f. field strength for a given pulse length until ^{13}C–^{1}H J-couplings could be resolved. Values corresponding to a 60 kHz offset were used. Settings were verified by performing ^{1}H–^{15}N SLF experiments on crystalline, acetylated ^{15}N-leucine. For correctly adjusted PMLG, the strongest modulation of the dipolar evolution curves was obtained.

All ^{13}C spectra of *polyethylene* were recorded at a temperature of T = 285 K. For cross polarization, a ^{1}H 90° pulse of 4.5 μs and a ramped 30 kHz ^{1}H and 40 kHz ^{13}C spin lock field was applied. Proton decoupling at 56 kHz was achieved using two pulse phase modulation (Bennett et al. 1995). The recycle delay time was 2 s. MAS experiments on ordered and powder samples were carried out at 5,000 Hz spin rate. In the SLF experiments, a ^{13}C 180° refocusing pulse during t_1 of 12 μs was used. ^{1}H–^{1}H decoupling at 60 kHz offset was achieved by PMLG (Lee and Goldburg 1965; Vinogradov et al. 1999). Thirty-two increments with 64 scans were acquired over one rotor period of 200 μs. Exponential line-broadening of 150 Hz was applied in ω_2 prior to Fourier transformation. DECs were obtained by plotting the integrated peak intensities over the time period of one rotor period.

The MAS experiments on ordered and unordered samples of *Bacteriorhodopsin* were acquired at 253 K and 5,000 Hz spin rate. For cross polarization, a ^{1}H 90° pulse of 5.5 μs, a ramped 45 kHz ^{1}H and 40 kHz ^{13}C spin lock field was used. A ^{15}N 180° pulse of 7 μs, ^{1}H TPPM-decoupling of 55 kHz and ^{1}H–^{1}H PMLG decoupling at 60 kHz offset were applied in the SLF experiment. Nine increments with 20,000 scans each were acquired over one rotor period of 200 μs. Exponential line-broadening of 25 Hz was applied prior to zero filling and Fourier transformation. The DECs of the respective ^{15}N nuclei are extracted by fitting Gaussian line-shapes to every ^{15}N resonance in each t_1 increment and plotting their intensities over the course of one rotor period.

Sample preparation

Highly ordered *polyethylene* can be obtained by macroscopically drawing the polymer into long fibers, in which the carbon chains adopt an all-*trans* conformation (Fig. 2a) (Graf et al. 1997; Opella and Waugh 1977; Schmidt-Rohr et al. 1992; Schmidt-Rohr and Spiess 1991; Schnell et al. 2001). The samples, a generous gift from Dr. I. Schnell and Dr. H. W. Spiess, consisted of teflon wrapped packets of aligned fibers. PE packages were carefully inserted into a 7 mm MAS zirconium rotor, with the fibers pointing along the rotor axis ($Z_D \parallel Z_R$), or perpendicular to the rotor axis ($Z_D \perp Z_R$), as schematically depicted in Fig. 2a. For powder measurements, PE fibers were cut up and ground with a mortar prior to packing into a 7 mm MAS rotor.

Bacteriorhodopsin Selectively ^{15}N-Methionine labeled bacteriorhodopsin (purple membrane) in its dark adapted state was prepared as described

previously (Mason et al. 2005). Oriented samples were obtained by spreading purple membrane (0.2 mg/25 µl buffered in D_2O) evenly over 47 glass discs with 0.07 mm thickness and 5.4 mm diameter (Marienfeld GmbH, Lauda-Königshofen, Germany). Excess water was allowed to evaporate over a period of 2 days at 91% air humidity at room temperature. The discs were stacked into a 7-mm MAS rotor and further hydrated over a period of ca. 4 days by placing a drop of saturated KNO_3 solution in the cap of the MAS rotor. Well-hydrated, uniaxially oriented films of purple membrane were obtained. The alignment process as well as adhesion of samples to the glass plates under MAS conditions was monitored with static ^{31}P NMR (not shown). A total amount of 9.5 mg purple membrane was used. D_2O was needed to remove peak overlap resulting from small contributions from loop and surface exposed residues (Mason et al. 2005).

Unordered (''powder'') samples were pelleted from distilled water and centrifuged into either 7 or 4 mm MAS rotors. The arrangement of the BR MAOSS sample is depicted schematically in Figs. 1b and 2b.

Computational details: numerical simulations of partially ordered samples

NMR spectra of powder samples are a superposition of signals stemming from a manifold of different molecular orientations. Therefore, numerical simulations of NMR powder spectra are time consuming as many different molecular orientations have to be averaged. The same applies to partially ordered samples where a numerical average over the appropriate orientation distribution has to be carried out. Significant progress has been made in making simulations of powder spectra as time efficient as possible by searching for the smallest set of Euler angles which approaches a full powder average. A number of schemes such as REPULSION (Bak and Nielsen 1997), ZCW (Zaremba (Zaremba 1966), Conroy (Conroy 1967) and Wolfsberg (Cheng et al. 1973)) or the computation of orientational averages developed by Levitt et al. (Eden and Levitt 1998) have been suggested. Here, we develop an algorithm which allows time efficient numerical simulations of NMR spectra for uniaxially ordered samples with a certain degree of mosaic spread as illustrated in Figs. 3 and 4. Our approach is based on the transformation of a given set of Euler angles for powder averaging into a set of angles corresponding to the orientation distributions found in uniaxially aligned samples.

In general, the FID observed for a powder may be described by Eq. 1 (Mehring 1983; Schmidt-Rohr and Spiess 1994).

$$s(t) = \frac{1}{8\pi^2}\int_0^{2\pi} \mathrm{d}\alpha_{\mathrm{PL}} \int_0^{\pi} \mathrm{d}\beta_{\mathrm{PL}} \sin\beta_{\mathrm{PL}} \int_0^{2\pi} \mathrm{d}\gamma_{\mathrm{PL}} s(t;\Omega_{\mathrm{PL}}). \qquad (1)$$

The Euler angles $\Omega_{\mathrm{PL}} = \{\alpha_{\mathrm{PL}}, \beta_{\mathrm{PL}}, \gamma_{\mathrm{PL}}\}$ denote the transformation of the principle axis frame P into the laboratory frame L defined by B_0. The FID $s(t; \Omega_{\mathrm{PL}})$

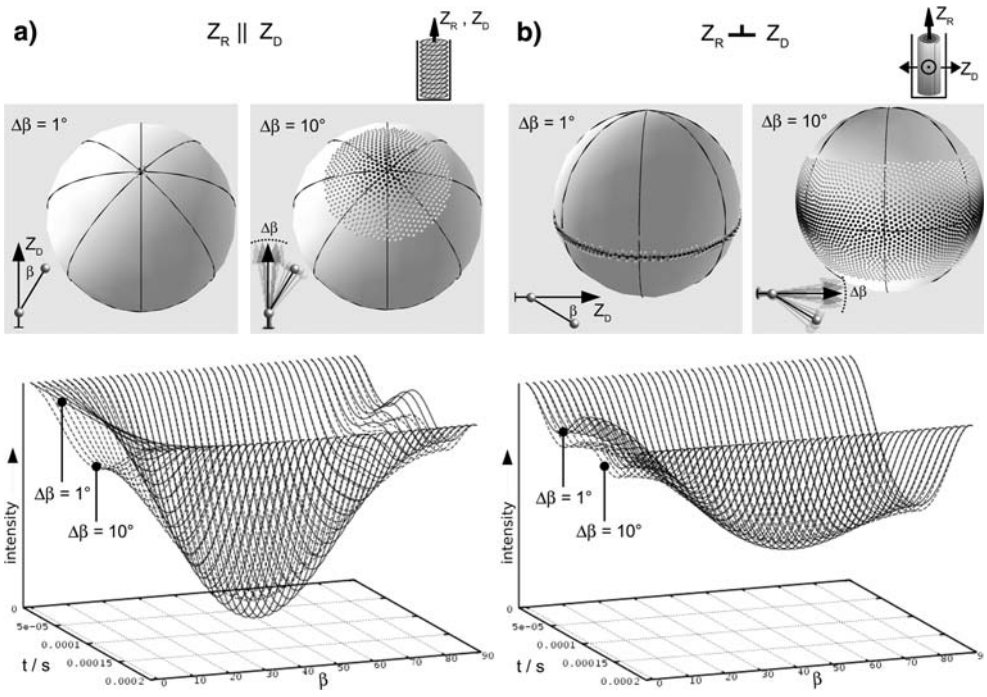

Fig. 4 Illustration of the sets of Euler angles $\{\alpha_{\mathrm{MD}}^{ij}, \beta_{\mathrm{MD}}^{ij}\}$ used to simulate samples with $Z_D \| Z_R$ (**a**) and $Z_D \perp Z_R$ (**b**) with different degrees of mosaic spread $\Delta\beta$. Each pair is represented by a dot on the sphere surface with the weighing factor $\omega_{ij}^{\mathrm{mos}}$ represented by the dot shading. Dipolar evolution curves were calculated in dependence of β for $Z_D \| Z_R$ (**a**) and $Z_D \perp Z_R$ (**b**). An increase of $\Delta\beta$ causes in both cases a flattening of the three-dimensional profile. The dipolar profile for $Z_D \perp Z_R$ is less pronounced as the molecules in the sample approach a pseudo powder distribution with increasing β. For these simulations, a sample spinning rate of 5,000 Hz and a ^1H–X dipolar coupling of 6,400 Hz was used

describes the time evolution for a single crystal whose orientation relative to the laboratory reference frame is specified by α_{PL}, β_{PL} and γ_{PL}. By using a finite number of crystallite orientations, Eq. 1 may be approximated by a discrete sum (Bak and Nielsen 1997):

$$\bar{s}(t) = \sum_{i=1}^{N}\sum_{j=1}^{M} s\left(t; \alpha_{PL}^{ij}, \beta_{PL}^{ij}\right)\omega_{ij} \tag{2}$$

In Eq. 2, ω_{ij} denotes a weighing factor which is assigned to each $\{\alpha_{PL}^{ij},\ \beta_{PL}^{ij}\}$ pair. It is meant to compensate for any non-uniformity in the distribution of a set of coordinates over a sphere, and fulfills the condition $\sum_{i=1}^{N}\sum_{j=1}^{M}\omega_{ij} = 1$. It is necessary to introduce coordinate transformations from the principal axis system P via the molecular frame M and/or sample director frame D into the laboratory frame L or the MAS rotor frame R as illustrated in Fig. 2. For the situation of ordered samples considered here, averaging takes place from M to D with a set of Euler angles $\{\alpha_{MD}^{ij},\ \beta_{MD}^{ij}\}$ and an appropriate weighing factor.

In order to approximate an ordered sample, we assume that the residual sample disorder corresponds to a Gaussian distribution (Nevzorov et al. 1999; Quine and Cross 2000) of the local director normal with a full width at half maximum given by the mosaic spread $\Delta\beta$. In order to create sets of Euler angles $\{\alpha_{MD}^{ij},\ \beta_{MD}^{ij}\}$ for the calculation of NMR spectra, we make use of an existing set of angles for a powder distribution and multiply the weighting factors for each α_{MD}^{ij}, β_{MD}^{ij} pair with a function describing a Gaussian distribution. For the geometry of the ordered sample considered here, the mosaic weighing factor is dependent only on the angle β_{MD}^{ij}, whereas the angle α_{MD}^{ij} may be neglected:

$$\omega_{ij}^{mos}\left(\beta_{MD}^{ij}, \Delta\beta\right) = \omega_{ij}\exp\left(-\frac{{\beta_{MD}^{ij}}^2}{2\Delta\beta^2}\right) \tag{3}$$

In order to minimize calculation time yet maintain an accurate approximation of our aligned sample, all coordinate pairs for which β_{MD}^{ij} is larger than $3\Delta\beta$ are discarded. For this condition, 99.7% of the crystallite coordinates which ''reside'' beneath the Gaussian curve which approximates the mosaic spread are included, and we assume that any crystallite coordinate which lies outside this range will have a negligible impact on the spectrum as a whole, due to its small weighing factor. In practice, this means that any coordinates with weighing factors ω_{ij}^{mos} are discarded if the condition expressed in Eq. 4 holds:

$$\omega_{ij}^{mos} \leq \omega_{ij}\exp\left(-\frac{9.0}{2.0}\right) = 0.011\omega_{ij} \tag{4}$$

In an effort to graphically represent these angle sets intuitively, we place, on the surface of a sphere, a rod at each coordinate $(\alpha_{MD}^{ij},\ \beta_{MD}^{ij})$ with a length which represents the weighing factor ω_{ij}^{mos} (Fig. 3). A powder crystal file of 1,000 coordinates, calculated with the REPULSION algorithm, is depicted in Fig. 3a. To the naked eye, all weighing factors (rod lengths) are very similar. The coordinates have been spread out on the crystal sphere in a largely uniform manner characteristic for the REPULSION algorithm (Bak and Nielsen 1997). The orientational distribution of ordered samples with $Z_D \| Z_R$ as shown in Fig. 1b is approximated by a crystal file with a ''shape'' which is reminiscent of a Gaussian (Fig. 3b) which is tilted by 90° if $Z_D \perp Z_R$ (Fig. 3c). If the sample shows additional carousel symmetry (Fig. 1c) a crystal file of the form shown in Fig. 3d is obtained.

Using appropriate simulation software such as SIMPSON (Bak et al. 2000), dipolar evolution curves can now be simulated for different orientation distributions according to

$$\begin{aligned}&\bar{s}(t, \beta, \alpha_{DR}, \beta_{DR}, \Delta\beta, \nu_{XH}, \nu_R)\\ &= \sum_{i=1}^{N}\sum_{j=1}^{M} s\left(t, \beta, \Delta\beta, \alpha_{DR}^{ij}, \beta_{DR}^{ij}, \nu_{XH}, \nu_R\right)\omega_{ij}^{mos}\end{aligned} \tag{5}$$

where β_{PD} is the tilt angle of the X–H dipolar coupling with respect to the director frame D, $\Delta\beta$ is the mosaic spread, ν_{XH} is the dipolar coupling, and ν_R the sample spinning speed. The angles α_{DR}, β_{DR} describe the orientation of the sample within the MAS rotor ($Z_D \perp Z_R$ or $Z_D \| Z_R$). We will refer to the tilt angle β_{PD} in the following as β.

The powder file which was used to calculate the MAOSS crystal files was calculated using the REPULSION algorithm (Bak and Nielsen 1997), but it is worth noting the other algorithms mentioned before may have advantages with respect to shorter calculation times (Cheng et al. 1973; Conroy 1967; Eden and Levitt 1998; Zaremba 1966). A set of MAOSS crystal files for the geometries considered here were calculated for a number of mosaic spread values $\Delta\beta$ in the range of 1–45° and used for fitting experimental DECs. Before implementing the crystal files in MAOSS-SLF calculations, they were tested extensively with the help of spectral simulations of static CSA spectra for various values of $\Delta\beta$ (data not shown).

Software

All simulations were carried out using SIMPSON 1.1.0 (Bak et al. 2000). Experimental dipolar evolution curves were fitted using MINUIT (James and Ross 1975), which was accessible via an interface implemented into SIMPSON by its creators (Vosegaard et al. 2002). Powder crystal files were calculated with the REPULSION program (Bak and Nielsen 1997). The calculations of crystal files for ordered samples were carried out with the help of the scripting languages Tcl 8.4 (Welch and Jones 2003), Gawk 1.3 (Dougherty and Robbins 1997) and Python 2.4 (Harms and McDonald 1999), as described before. Graphs were created with the open-source plotting program Gnuplot 4.0 (Williams and Kelley 2004). Visualizations of the orientational distribution in Figs. 3–5 were carried out with the help of Python 2.4, and its module ''visual'', also known as ''VPython'' (Roberts et al. 2004; Scherer et al. 2000). All software is open source and is available for free download on the internet.

Results and discussion

Simulation of SLF experiments for samples with different orientational distributions

Using the simulation procedure described before, we have calculated dipolar evolution curves for samples with $Z_D \| Z_R$ as well as for samples with $Z_D \perp Z_R$ and additional carousel symmetry (Fig. 1). Simulations were carried out for a mosaic spread $\Delta\beta = 1°$ and 10°. The dipolar tilt angle β was varied between 0° and 90°. A sample spin rate of 5,000 Hz was used and a ^1H–^{15}N dipolar coupling of 6,400 Hz assumed. This coupling value is close to the values found for peptidic ^1H–^{15}N dipolar interactions (~11,300 Hz (Bak et al. 2002)), after being scaled by 57%, due to Lee Goldburg decoupling. The appropriate sets of Euler angles $\{\alpha_{MD}^{ij}, \beta_{MD}^{ij}\}$ are shown with the calculated dipolar evolution curves in Fig. 4. The $\{\alpha_{MD}^{ij}, \beta_{MD}^{ij}\}$ sets are represented graphically by dots which reside on the surface of a sphere and are shaded according to the Euler angle pair's weighing factor ω_{ij}^{mos}.

For $Z_D \| Z_R$ (e.g. the stacked disc setup in Fig. 1b) the graphical representation of the appropriate crystal file shows that the crystallites are clustered in a circular arrangement around the upper pole of the sphere. The weighing factors are highest at the top center of the sphere, and diminish with rising distance from the spheres upper pole. An increase in mosaic spread is described by a wider distribution of $\{\alpha_{MD}^{ij}, \beta_{MD}^{ij}\}$ with an appropriate weighing factor calculated according to Eq. 2 (Fig. 4a). Using these Euler angle sets, DECs have been calculated for $\Delta\beta = 1°$ and $\Delta\beta = 10°$ with β values ranging between 0° and 90° (Fig. 4a). At $\beta = 0°$, the internuclear vector lies along the MAS rotor axis, at the magic angle to B_0, and the dipolar couplings collapse to zero. Consequently, the DEC consists of a straight line and displays no modulation. At an angular value of $\beta = 90°$, the DEC displays a double periodicity which is due to the $\sin 2\beta$ and $\sin^2\beta$ orientation dependence of the ω_r and $2\omega_r$ rotor-modulated terms of the MAS interaction Hamiltonian (Fischbach et al. 2004; Maricq and Waugh 1979; Mehring 1983). The strongest modulation is seen at 45°. Increasing mosaic spread causes a general flattening of the 3D plot in Fig. 4a which results in poorer angle resolution.

The Euler angle sets for samples with $Z_D \perp Z_R$ and additional carousel symmetry around Z_R (e.g. samples aligned on cylindrical polymer films as shown in Fig. 1c) cover a larger area along the equator for the same mosaic spread compared to samples with $Z_D \| Z_R$ (Fig. 4b). The dipolar evolution curve for $\beta = 0°$ shows a double periodicity as the H–X vector is perpendicular to Z_R. With increasing β, a pseudo powder distribution is approached. Therefore, the three-dimensional DEC profile for $Z_D \perp Z_R$ is less pronounced than for $Z_D \| Z_R$. An increasing mosaic spread causes an additional general flattening here as well. It should be mentioned that these conclusions apply also to samples with $Z_D \perp Z_R$ which do not feature carousel symmetry around Z_R (e.g. plates in Fig. 1c or PE in Fig. 2a) if data acquisition is not synchronized with the rotation of the sample.

^{13}C–^1H-SLF experiments on ordered polyethylene

To test experiments and simulations, we have used ordered samples of polyethylene which is a very well characterized polymer. The orientation of the C–H dipolar couplings with respect to the axis of molecular order (Fig. 2a) is known. Controlling the orientation of this axis with respect to Z_R can be easily achieved by placing ordered PE parallel or perpendicular into the MAS rotor. This should result in modulations of the C–H dipolar evolution curves, which allows verification of the described procedures.

First, SLF experiments were carried out on unordered samples in order to determine the C-H dipolar coupling which is needed for the subsequent analysis of ordered samples. A value of 12,236 Hz was obtained. The unscaled dipolar couplings of ^1H–^{13}C nuclei have a value of ~22 kHz (Schmidt-Rohr et al. 1993). Homonuclear ^1H–^1H PMLG decoupling introduces a dipolar

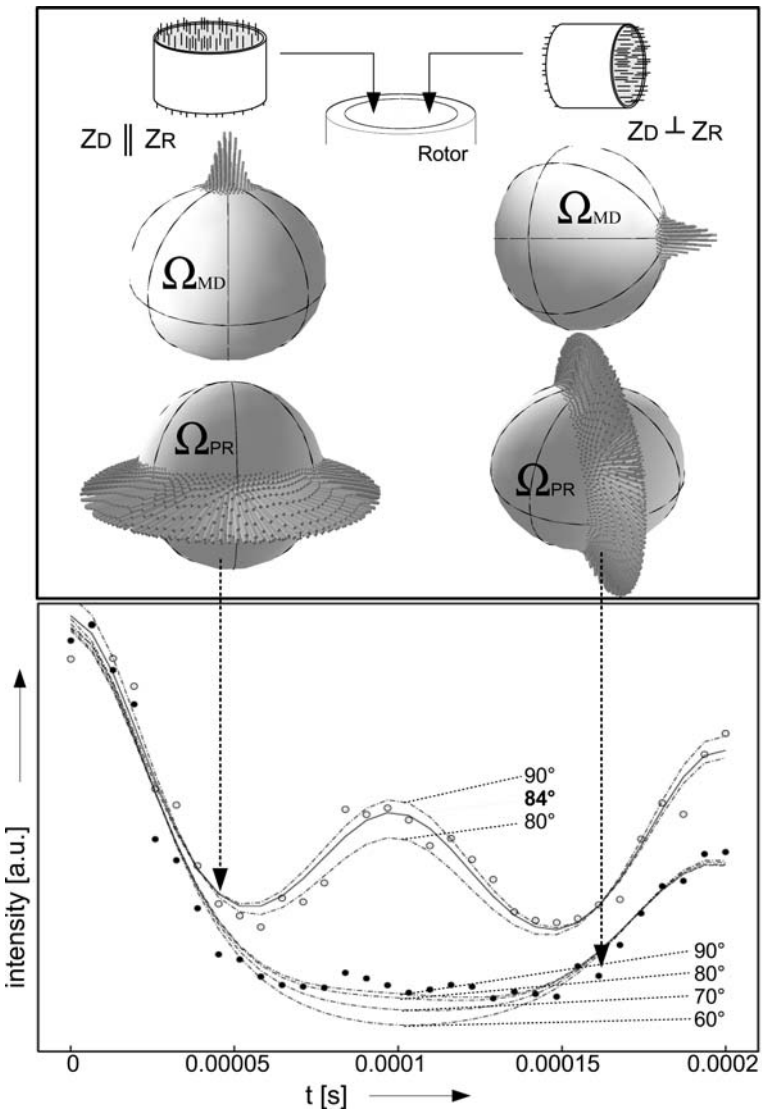

Fig. 5 The actual orientation distribution of the C–H vectors within the MAS rotor frame is illustrated at the top, and measured and simulated dipolar evolution curves for ordered PE fibers which were placed parallel or perpendicular into a MAS rotor are displayed at bottom. The double periodicity for $Z_R \| Z_D$ is caused by the nearly perpendicular orientation of the C–H vector with respect to Z_D which also explains the pseudo powder distribution observed for $Z_D \perp Z_R$ Simulation details are summarized in Table 1

scaling factor of 57% (Lee and Goldburg 1965), resulting in a value of ~12,540 Hz, which compares well with our result.

The quality (mosaic spreads) of the PE sample orientation was estimated by fitting the line-shape of static ^{13}C-CP spectra of PE as a function of the mosaic spread $\Delta\beta$ (not shown). The values for the isotropic chemical shift, the chemical shift anisotropy as well as the asymmetry parameter η were obtained by analyzing static and MAS powder spectra and correspond well to those found in literature (literature values in brackets: δ =31 ppm (30 ppm), CSA = 19.95 ppm (20 ppm), η = 0.73 (0.7)) (Fischbach et al. 2004).

The orientation distribution of the carbon chains within drawn PE fiber samples is known to have a spread of $\Delta\beta = 8°$ (Fischbach et al. 2004). We take this to be the lowest possible intrinsic value for the mosaic spread of the oriented PE samples used here. Indeed, the ^{13}C 1D NMR fits to the experimental results give respective mosaic spreads of $\Delta\beta = 10°$ for the case where $Z_R \| Z_D$ and $\Delta\beta = 16°$ for $Z_R \perp Z_D$.

The DECs of the PE samples, oriented in the two described different directions, were fitted by varying the angle β and the relaxation $(1/T_2^*)$ iteratively. Results are summarized in Table 1 and shown in Fig. 5.

Due to the shape of the MAOSS crystal files and the molecular geometry of our sample (the ^{13}C–^{1}H dipolar vectors lie in planes which are perpendicular to the axis Z_M, see Fig. 2), β-values in the vicinity of 90° are expected. The best fits for the respective DECs are obtained for angular values of $80° \leq \beta \leq 90°$ ($Z_R \| Z_D$) and $60 \leq \beta \leq 90$ ($Z_R \perp Z_D$).

The accuracy for β in the 90° region is much higher for $Z_R \| Z_D$ compared to $Z_R \perp Z_D$ as shown in Fig. 4.

Table 1 Fit results for polyethylene MAS and MAOSS measurements in the unordered state and in two differently oriented ordered states (see text for details)

Powder		Oriented: Z_D parallel Z_R			Oriented: Z_D perpendicular Z_R		
dc [Hz]	Lb [Hz]	$1/T_2^*$ [Hz]	β [°]	$\Delta\beta$ [°]	$1/T_2^*$ [Hz]	β [°]	$\Delta\beta$ [°]
12,236	368	588	85 ± 5	10	1,275	75 ± 15	16

Therefore, both results agree with each other and are close to the expected value within the error range. The poorer accuracy of the measurement of the second sample is also connected to its larger mosaic spread which can be explained by difficulties in aligning it within the MAS rotor. The insertion of the fiber bundle into the MAS rotor was simpler for the parallel than for the perpendicular case (Fig. 2).

In general, the results for the β angles, dipolar couplings and mosaic spreads $\Delta\beta$ agree with the values expected, and verify the experimental approach and our method of data analysis. It can also be concluded from these data, that a sample alignment with $Z_R \| Z_D$ allows more accurate measurements over a wider angle range.

What is the best sample geometry for SLF experiments on bacteriorhodopsin?

Samples of purple membrane can be aligned on a solid support which is placed into a MAS rotor. As mentioned before three different sample geometries have been suggested as illustrated in Fig. 1. Alignment on glass plates which are placed with $Z_D \perp Z_R$ into a MAS rotor results in a poor sample filling factor and is not ideal for sample spinning. Therefore, we limit our attention to the alignment on glass plates with $Z_D \| Z_R$ (Glaubitz and Watts 1998) and on rolled polymer films with $Z_D \perp Z_R$ (Sizun and Bechinger 2002). Both geometries have been already discussed above with respect to suitable sets of Euler angles $\{\alpha_{MD}^{ij}, \beta_{MD}^{ij}\}$ and SLF experiments. The three-dimensional DEC profile in Fig. 4 is more pronounced for the disk setup compared to the film geometry as the orientational distribution function of ^{1}H–X dipolar couplings approaches quickly a pseudo-powder with increasing β or $\Delta\beta$. In order to compare the two experimental setups, it is convenient to view our graphs as valleys which possess a certain depth and a certain slope which are indicative of the sensitivity of the experiment to changes in the angular values β. A steep slope and a deep valley indicate a high sensitivity of the DEC to changes in the angle β. This view is best quantified by numerical differentiation of the DEC intensity with respect to the angle β. In order to gauge the effect of the mosaic spread, the differentiation was carried out for a range of values for the mosaic spread $\Delta\beta$, ranging from 1° to 45°, as depicted in Fig. 6. The result indicates that the highest rate of change in the SLF modulation occurs for values ranging from 15° to 35°, and for values ranging from 55° to 75°. With large mosaic spreads, the sensitivity is lowered drastically, as the angular dependence disappears, due to the loss in macroscopic orientation of the sample.

Perhaps the most interesting result which is highlighted in Fig. 6 is that experiments which utilize the disc setup show a response to changes in the angle β which is twice as sensitive to that of the film geometry.

Conclusively, alignment on discs with $Z_D \| Z_R$ is more sensitive to changes in the angular value of β than alignment on rolled films with $Z_D \perp Z_R$. It is also less susceptible to the effect of the mosaic spread, and last but not least takes less calculation time due to a smaller number of necessary crystallite coordinates. Consequently, we have used the geometry depicted in Fig. 1b in order to demonstrate the measurement of the orientation of ^{1}H–^{15}N dipole couplings in BR.

^{15}N–^{1}H-SLF experiments on bacteriorhodopsin

The one-dimensional ^{15}N-CP-NMR spectra of ^{15}N-Met purple membranes exhibit five clearly resolved peaks (1D MAOSS spectrum, Fig. 7a). The assignments of methionines 20, 32, 56, 60, 118, 145 and 209 are indicated in Fig. 7a, and are taken from previous work (Mason et al. 2005). It should be noted that, in an effort to avoid spectral overlap, rehydration of the sample was carried out with buffered D_2O and lead to the deuterium exchange for the amide protons of methionines 68, 163 and 32, which reside at the bilayer interface to the aqueous phase (Mason et al. 2005).

Data analysis was restricted to the DECs of methionines 20, 118 and 145. Methionines 56, 60 and 209 are omitted from further discussion, because attempts to fit the DECs of these amino acid residues were thwarted, due to a strong overlap of their signals. The measured (circles) and calculated (lines) DECs for methionines 20, 118 and 145, for unordered and strongly oriented samples, are depicted in Fig. 7b.

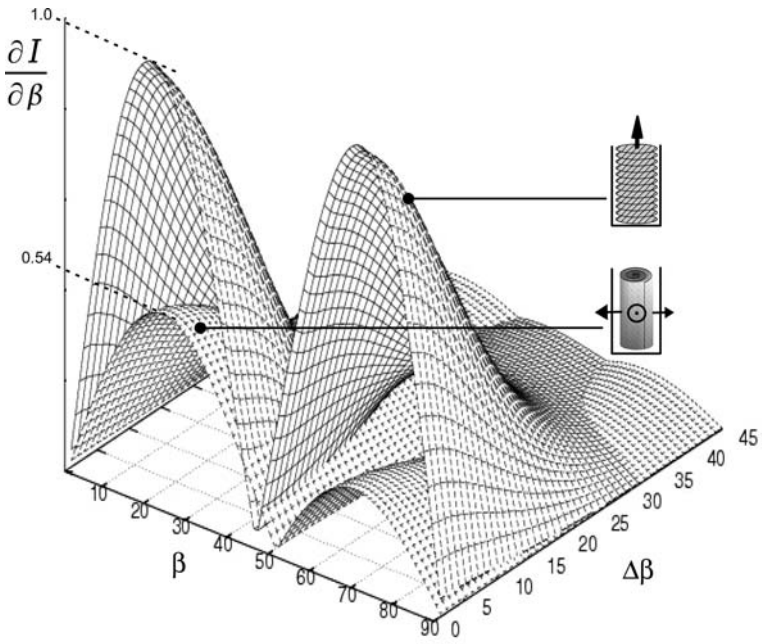

Fig. 6 The response of dipolar evolution curves to changes of the angle β is visualized by plotting $dI/d\beta$ (for $t = \tau_R/2$) as a function of β and $\Delta\beta$. Both experimental setups depicted in Fig. 1 are considered. Highest angle resolution is achieved between 10° and 35° and 55° and 75°. It is worth noting that SLF measurements on samples with $Z_D \| Z_R$ are roughly twice as sensitive to changes in β as the samples with $Z_D \perp Z_R$

Best fits of the DECs for methionines 20 and 118 in the unordered state were calculated for (scaled) dipolar coupling values of 6,466 Hz (methionine 20) and 6,534 Hz (methionine 118). The use of Lee–Goldburg proton–proton decoupling scales the dipolar coupling down by 57% (Lee and Goldburg 1965) which agrees well with an unscaled dipolar coupling of 11,341 Hz for a ^{15}N–^{1}H nuclear peptide pair (Bak et al. 2002).

Best fit results of the DECs for methionines 20, 118 and 145 in the oriented samples were obtained with the values for the angles β, mosaic spreads $\Delta\beta$ and T_2^* relaxation which are listed in Table 2. The accuracy of these measurements is generally better compared to the values obtained for PE, as the angles are found within the most sensitive range of the SLF experiment.

The orientation of N–H couplings is in a range expected for transmembrane α-helices and reflects their tilt and pitch angle. A detailed discussion in the light of a number of very well resolved 2D and 3D crystal structures of BR (Luecke et al. 1999; Subramaniam and Henderson 2000) is beyond the scope of this paper, however, a simple analysis indicates that our results are correct: As coordinates for protons cannot be obtained from X-ray data, we have measured the angle between different O_{i-4}, N_i vectors of Gly16, Met20 and Thr114, Met118 in 1C3W (Luecke et al. 1999). This approximation is possible due to the linear character of NH...O hydrogen bonds. The crystal coordinates indicate that the angle subtended by the two vectors is 150°. The angle measured by our NMR approach corresponds to the opening angle of a cone described by the N–H vector. Considering the in-plane position of both vectors, our data corresponds to possible difference angles of 9°, 29°, 152° and 170° (see Table 3). The third value agrees very well with the angle taken from the crystal file. The reason for finding four possibilities is caused by the two-dimensional character of our samples and the symmetry of NMR interactions around β_{PR} or $\beta_{PL} = 90°$. The same applies for Met 145 tilt angles as well (Table 3).These data are very consistent with the tilt angles obtained from the X-ray structure.

A further comparison is possible with direct measurements of ^{15}N–^{1}H dipolar couplings obtained by PISEMA experiments on bacteriorhodopsin with identical ^{15}N-Met isotope labeling (Kamihira et al. 2005). The PISEMA measurements used in this study showed that the dipolar couplings of the helical methionines are to be found for values ranging from 7 kHz to 10 kHz (Kamihira et al. 2005). A simple calculation shows that our measured angles for methionines 20, 118 and 145 correspond to dipolar coupling values of 10, 8.8 and 10 kHz, respectively, which lie within these boundaries.

The main difference between fully anisotropic SLF experiments on ordered samples (such as PISEMA) and the MAOSS-SLF approach presented here lies in the fact that the ^{1}H–^{15}N dipolar coupling is correlated to the ^{15}N isotropic shift, and not to the CSA. Theoretically, for the MAOSS SLF experiment, this would result in a loss of resolution in the ^{15}N dimension, due to a refocusing of ca. 220 ppm CSA into the isotropic chemical shift dispersion (ca. 20 ppm). However, the significantly sharper spectral resolution of the MAOSS measurements can compensate for this: Residual

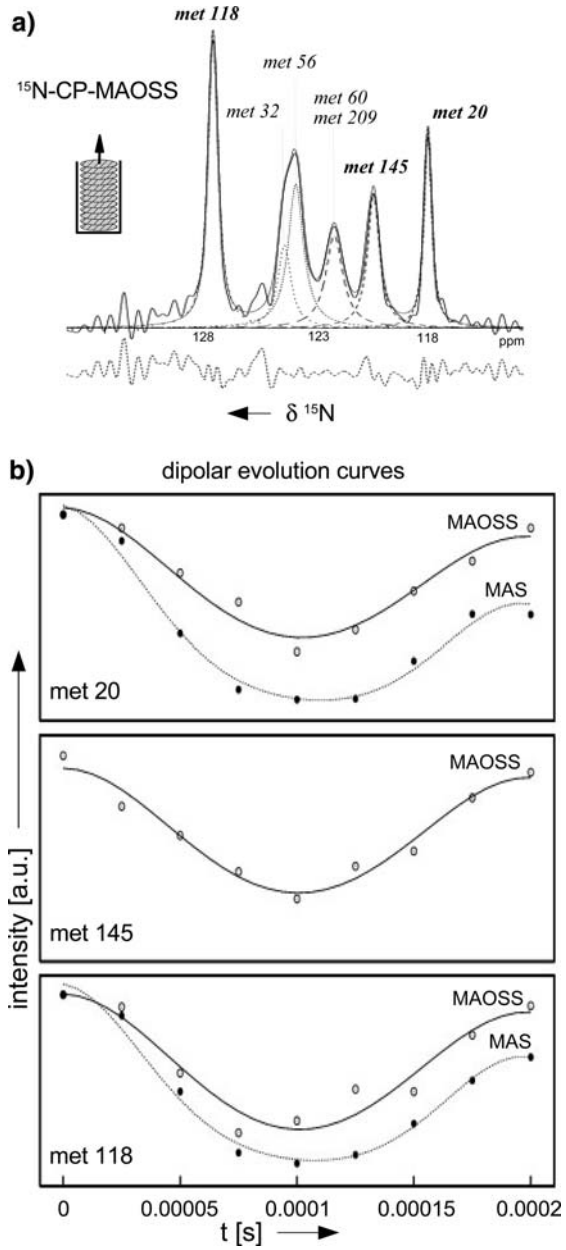

Fig. 7 Bacteriorhodopsin MAOSS measurements: (**a**) 1D ^{15}N-CP-MAOSS spectrum on strongly aligned ^{15}N-met bR samples. The signals of methionines 20, 118 and 145 are clearly discernible and were used for further analysis. Signal intensities were obtained by spectral deconvolution with the fit of seven Gaussian peaks to the 1D slice of each increment. The residual (difference between measured and calculated lineshapes) is included beneath the spectrum. (**b**) Dipolar evolution curves for unordered (MAS) and ordered (MAOSS) samples, calculated and experimental, for the amide nitrogens of the methionine residues 20, 118 and 145

disorder can cause severe linebroadening ($\Delta\nu_{1/2} \approx$ 50 ppm) in the static case, as seen for ^{15}N-Met bacteriorhodopsin (Kamihira et al. 2005; Mason et al. 2004),

Table 2 Fit results for samples of ordered and unordered samples of bacteriorhodopsin MAS and MAOSS measurements (see text for details)

Residue	Powder		Oriented		
	dc [Hz]	$1/T_2^*$ [Hz]	β [°]	$\Delta\beta$ [°]	$1/T_2^*$ [Hz]
Met 20	6,466	430	10 ± 2	13	115
Met 118	6,534	325	19 ± 2	8	76
Met 145	–	–	10 ± 2	14	37

but is refocussed under MAS ($\Delta\nu_{1/2} \approx$ 1 ppm), allowing, for example, the resolution and assignment of six out of the nine residues (Mason et al. 2005).

A correct data analysis needs including parameters for the mosaic spread as discussed before. A direct measurement of the mosaic spread is difficult in case of the purple membrane samples used here: Static ^{31}P NMR cannot be used to report on the lipid headgroup alignment as there are no bulk lipids. Static ^{15}N NMR cannot be used directly as it is not possible to align the MAS rotor with $Z_R \| B_0$. However, the mosaic spreads which result from our data analysis are comparable to values from static experiments found for almost identical samples (Mason et al. 2004). Methionine 118 ($\Delta\beta$ = 8°) seems to have a much smaller value than methionines 20 and 145 ($\Delta\beta$ = 13° and 14°, respectively). Such variations in mosaic spread between different sites are possible, due to differences in conformational heterogeneities. It is noteworthy that simulations and fitting in which the mosaic spread was set to different constant values did not result in different values for the angle β.

Conclusion

Here, we have shown that SLF-MAS experiments on ordered samples can provide the orientations of ^{1}H–^{13}C and ^{1}H–^{15}N bond vectors within the MAS rotor. The angle β, spanned by the bond vector and z-axis of the rotor is obtained by simulating experimental results. The orientation distribution of these bond vectors due to residual disorder (mosaic spread) and two-dimensional distributions within the sample are accounted for by calculating a set of Euler angles with appropriate weighing factors. This novel procedure can be applied to any situation in which NMR experiments on partially ordered samples have to be analyzed.

Computer simulations revealed, that samples in which the axis of molecular order (Z_D) is placed parallel to the rotor axis (Z_R) allow a higher β angle resolution compared to other arrangements. The SLF experiments presented here are only sensitive to β not

Table 3 Comparison of angle measurements with data obtained from the 1.5 Å X-ray structure (1C3W)

Residues		X-ray		MAOSS-SLF NMR
i	j	Dihedral angle (O_{i-4}–N_i – N_j–O_{j-4})	Tilt angles (N_i–O_{i-4}), (N_j–O_{j-4})	Angle differences (N_iH_i), (N_jH_j)
Met 20	Met 118	164°[a]	150°[a]	9, 29, 151, 170
Met 20	Met 145	15°[b]	22°[b]	0, 20, 160, 180
Met 118	Met 145	168°[c]	169°[c]	9, 29, 151, 170

The angle differences of (N_i–O_{i-4}) and (N_j–O_{j-4}) vectors are consistent with the allowed angle differences of (N_iH_i) and (N_jH_j) vectors obtained by NMR. (a) i-4 = Gly 16, i = Met 20, j = Met 118, j-4 = Ala 114; (b) i-4 = Gly 16, i = Met 20, j = Met 145, j-4 = Ser 141; (c) i-4 = Ala 114, i = Met 118, j = Met 145, j-4 = Ser 141 (see text for details)

α due to the effective carousel symmetry of our samples around the rotor axis. However, using rotor-synchronized data acquisition with samples which have a unique orientation Ω_{DR} with respect to the rotor, both α and β could be determined (Gross et al. 2005).

Our theoretical predictions and experimental procedures have been verified by determining the orientation of C–H dipolar couplings in CH_2 groups of polyethylene which serves as a well characterized model system (Fischbach et al. 2004). For a more realistic demonstration, the 26 kDa membrane protein bacteriorhodopsin has been chosen. We have determined N–H bond orientations of three labeled residues which had been previously assigned. The alignment of purple membrane on glass plates with $Z_D \| Z_R$ is preferred over the use of polymer films due to a superior angle resolution. The film setup has advantages with respect to the ability to use smaller MAS rotors and higher sample spinning speed, although this has no relevance in the case of the SLF experiments suggested here, as lower spinning speeds are needed.

It is important to discuss the approach suggested here in the light of established experiments which are fully anisotropic, do not require sample spinning and could have a less complicated molecular orientation distribution with respect to B_0, such as PISEMA experiments and their application to membrane samples with $Z_D \| B_0$. PISEMA experiments with high spectral resolution have been demonstrated on membrane samples aligned on glass plates and very promisingly on proteins incorporated into self-aligning bicells (De Angelis et al. 2004). But for the samples shown here the SLF-MAOSS experiment offers a better spectral resolution compared to PISEMA spectra of the same sample (Kamihira et al. 2005). In addition, only a small number of increments are needed as the dipolar evolution curve is sampled just over one rotor period. Of disadvantage is clearly the loss of one anisotropic dimension by correlating isotropic chemical shifts with dipolar couplings. Also, the analysis relies on a good signal-to-noise ratio and not on frequency measurements as in experiments on non-rotating samples. However, the use SLF experiments on ordered samples offers still interesting possibilities. The good spectral resolution even in samples with considerable disorder and the sensitive response to angle changes make it potentially very useful for the detection of structural changes associated for example with helix re-orientations. As indicated in Fig. 4, the DECs are very sensitive to small angular changes for β in the regions of 15–25° and 55–80°. Problems arising from spectral overlap in 1D ^{15}N spectra as shown in Fig. 7 could be overcome by correlating ^{15}N–^{1}H dipolar couplings with two-dimensional ^{15}N–^{1}H HETCOR spectra. Further experiments to explore this potential have been carried out on ^{15}N-Met-D85N/T170C mutants of bacteriorhodopsin which allow the generation of N- and O-like states (Mason et al. 2005) and will be reported elsewhere.

Acknowledgements We thank Dr. Ingo Schnell and Prof. H. W. Spiess for the generous gift of the polyethylene samples. Stimulating discussions with Prof. T. Vosegaard and Prof. Niels Nielsen are gratefully acknowledged. The work was funded by the Deutsche Forschungsgemeinschaft.

References

Bak M, Nielsen NC (1997) REPULSION: a novel approach to efficient powder averaging in solid-state NMR. J Magn Reson 125:132–139

Bak M, Rasmussen JT, Nielsen NC (2000) SIMPSON: a general simulation program for solid-state NMR spectroscopy. J Magn Reson 147:296–330

Bak M, Schultz R, Vosegaard T, Nielsen NC (2002) Specification and visualization of anisotropic interaction tensors in polypeptides and numerical simulations in biological solid-state NMR. J Magn Reson 154:28–45

Bennett AE, Rienstra CM, Auger M, Lakshmi KV, Griffin RG (1995) Heteronuclear decoupling in rotating solids. J Chem Phys 103:6951–6958

Cheng VB, Suzukawa HH, Wolfsberg M (1973) Investigations of a nonrandom numerical method for multidimensional integration. J Chem Phys 59:3992–3999

Conroy H (1967) Molecular schrodinger equation 8. A new method for evaluation of multidimensional Integrals. J Chem Phys 47:5307

Cross TA, Quine JR (2000) Protein structure in anisotropic environments: development of orientational constraints. Conc Magn Reson 12:55–70

De Angelis AA, Nevzorov AA, Park SH, Howell SC, Mrse AA, Opella SJ (2004) High-rosolution NMR spectroscopy of membrane proteins in aligned bicelles. J Am Chem Soc 126:15340–15341

Dougherty D, Robbins A (1997) sed & awk. O'Reilly, Cambridge

Eden M, Levitt MH (1998) Computation of orientational averages in solid-state NMR by Gaussian spherical quadrature. J Magn Reson 132:220–239

Fischbach I, Ebert F, Spiess HW, Schnell I (2004) Rotor modulations and recoupling strategies in C-13 solid-state magic-angle-spinning NMR spectroscopy: probing molecular orientation and dynamics. Chem Phys Chem 5:895–908

Glaubitz C, Burnett IJ, Grobner G, Mason AJ, Watts A (1999) Deuterium-MAS NMR spectroscopy on oriented membrane proteins: applications to photointermediates of bacteriorhodopsin. J Am Chem Soc 121:5787–5794

Glaubitz C, Grobner G, Watts A (2000) Structural and orientational information of the membrane embedded M13 coat protein by C-13-MAS NMR spectroscopy. Biochim Biophys Acta Biomem 1463:151–161

Glaubitz C, Watts A (1998) Magic angle-oriented sample spinning (MAOSS): a new approach towards biomembrane studies. J Magn Reson 130:305–316

Graf R, Demco DE, Gottwald J, Hafner S, Spiess HW (1997) Dipolar couplings and internuclear distances by double-quantum nuclear magnetic resonance spectroscopy of solids. J Chem Phys 106:885–895

Gross BJ, Tanski JM, McDermott AE (2005) Structure determination of aligned systems by solid-state NMR magic angle spinning methods. J Magn Reson 176:223–233

Harms D, McDonald K (1999) The quick python book. Manning Publications Co., Greenwich Connecticut

Hester RK, Ackerman JL, Neff BL, Waugh JS (1976) Separated local field spectra in NMR—determination of structure of solids. Phys Rev Lett 36:1081–1083

James F, Ross M (1975) Minuit—a system for function minimization and analysis of the parameter errors. Comp Phys Comm 10:343

Kamihira M, Vosegaard T, Mason AJ, Straus SK, Nielsen NC, Watts A (2005) Structural and orientational constraints of bacteriorhodopsin in purple membranes determined by oriented-sample solid-state NMR spectrocopy. J Struct Biol 149:7–16

Lanyi JK, (2004) Bacteriorhodopsin. Annu Rev Physiol 66:665–688

Lee M, Goldburg WI (1965) Nuclear-magnetic-resonance line narrowing by a rotating Rf field. Phys Rev 140:1261

Luca S, White JF, Sohal AK, Filippov DV, van Boom JH, Grisshammer R, Baldus M (2003) The conformation of neurotensin bound to its G protein-coupled receptor. Proc Natl Acad Sci USA 100:10706–10711

Luecke H, Schobert B, Richter HT, Cartailler JP, Lanyi JK (1999) Structure of bacteriorhodopsin at 1.55 angstrom resolution. J Mol Biol 291:899–911

Mai W, Hu W, Wang C, Cross TA (1993) Orientational constraints as 3-dimensional structural constraints from chemical-shift anisotropy—the polypeptide backbone of gramicidin-a in a lipid bilayer. Protein Sci 2:532–542

Maricq MM, Waugh IS (1979) NMR in rotating solids. J Chem Phys 70:3300–3316

Mason AJ, Grage SL, Straus SK, Glaubitz C, Watts A (2004) Identifying anisotropic constraints in multiply labeled bacteriorhodopsin by N-15 MAOSS NMR: a general approach to structural studies of membrane proteins. Biophysics J 86:1610–1617

Mason Al, Turner GJ, Glaubitz C (2005) Conformational heterogeneity of transmembrane residues after the schiff base reprotonation of bacteriorhodopsin—N-15 CPMAS NMR of D85N/T170C membranes. FEBS J 272:2152–2164

Mehring M (1983) Principles of high resolution NMR of solids. Springer, New York

Moll F, Cross TA (1990) Optimizing and characterizing alignment of oriented lipid bilayers containing gramicidin-D. Biophys J 57:351–362

Munowitz MG, Griffin RG (1982) Two-dimensional nuclear magnetic-resonance in rotating solids—an analysis of lineshapes in chemical shiftdipolar spectra. J Chem Phys 76:2848–2858

Munowitz MG, Griffin RG, Bodenhausen G, Huang TH (1981) Two-dimensional rotational spin-echo nuclear magnetic-resonance in solids—correlation of chemical-shift and dipolar interactions. J Am Chem Soc 103:2529–2533

Nevzorov AA, Trouard TP, Brown MF (1999) Lipid bilayer dynamics from orientation and frequency dependent deuterium NMR relaxation. Biophys J 76:A441–A441

Nicholson LK, Moll F, Mixon TE, Lograsso PV, Lay JC, Cross TA (1987) Solid-sate N-15 NMR of oriented lipid bilayer bound gramicidin-A. Biochemistry 26:6621–6626

Opella SJ, Ma C, Marassi FM (2001) Nuclear magnetic resonance of membrane-associated peptides and proteins. Nucl Magn Reson Biol Macromol Pt B 339:285–313

Opella SJ, Waugh IS (1977) 2-Dimensional C-13 NMR of highly oriented polyethylene. J Chem Phys 66:4919–4924

Quine JR, Cross TA (2000) Protein structure in anisotropic environment: unique structural fold from orientational constraints. Conc Magn Reson 12:71–82

Ramamoorthy A, Opella SJ (1995) 2-Dimensional chemical-shift heteronuclear dipolar coupling spectra obtained with polarization inversion spin-exchange at the magic-angle and magic-angle sample-spinning (Pisemamas). Solid State Nucl Magn Reson 4:387–392

Rienstra CM, Hohwy M, Hong M, Griffin RG (2000) 2D and 3D N-15-C-13-C13 NMR chemical shift correlation spectroscopy of solids: assignment of MAS spectra of peptides. J Am Chem Soc 122:10979–10990

Roberts S, Gardner H, Press S, Stals L (2004) Teaching computational science using V Python and virtual reality. In Computational Science-ICCS 2004, Proceedings, vol 3039, pp1218–1225

Scherer D, Dubois P, Sherwood B (2000) VPython: 3D interactive scientific graphics for students. Comp Sci Eng 2:56–62

Schmidt-Rohr K, Hehn M, Schaefer D, Spiess HW (1992) 2-Dimensional nuclear-magnetic-resonance with sample flip for characterizing orientation distributions, and its analogy to X-ray-scattering. J Chem Phys 97:2247–2262

Schmidt-Rohr K, Spiess HW (1991) Chain diffusion between crystalline and amorphous regions in polyethylene detected by 2D exchange C-13 NMR. Macromolecules 24:5288–5293

Schmidt-Rohr K, Spiess HW (1994) Multidimensional solid-state NMR and Polymers. Academic Press, New York

Schmidt-Rohr K, Wilhelm M, Johansson A, Spiess HW (1993) Determination of chemical-shift tensor orientations in methylene groups by separated-local-field NMR. Magn Reson Chem 31:352–356

Schnell I, Watts A, Spiess HW (2001) Double-quantum double-quantum MAS exchange NMR spectroscopy:

dipolar-coupled spin pairs as probes for slow molecular dynamics. J Magn Reson 149:90–102
Sizun C, Bechinger B (2002) Bilayer sample for fast or slow magic angle oriented sample spinning solid-state NMR spectroscopy. J Am Chem Soc 124:1146–1147
Song XJ, Rienstra CM, McDermott AE (2001) N-H bond stretching in histidine complexes: a solid-state NMR study. Magn Reson Chem 39:S30–S36
Subramaniam S, Henderson R (2000) Molecular mechanism of vectorial proton translocation by bacteriorhodopsin. Nature 406:653–657
Ulrich AS, Watts A (1993) H-2 NMR lineshapes of immobilized uniaxially oriented membrane-proteins. Solid State Nucl Magn Reson 2:21–36
van Dam L, Levitt MH (2000) BII nucleotides in the B and C forms of natural—sequence polymeric DNA: a new model for the C form of DNA. J Mol Biol 304:541–560
Vinogradov E, Madhu PK, Vega S (1999) High-resolution proton solid-state NMR spectroscopy by phase-modulated Lee-Goldburg experiment. Chem Phys Lett 314:443–450
Vosegaard T, Malmendal A, Nielsen NC (2002) The flexibility of SIMPSON and SIMMOL for numerical simulations in solid- and liquid-state NMR spectroscopy. Monatsh Chem 133:1555–1574
Waugh JS (1976) Uncoupling of local field spectra in nuclear magnetic-resonance-determination of atomic positions in solids. Proc Natl Acad Sci USA 73:1394–1397
Welch BB, Jones K (2003) Practical Programming in Tcl and Tk. Prentice Hall, New Jersey
Williams T, Kelley C (2004) GNUPlot - an interactive plotting program.(www.gnuplot.info)
Wu CH, Ramamoorthy A, Opella SJ (1994) High-resolution heteronuclear dipolar solid-state NMR-spectroscopy. J Magn Reson Ser A 109:270–272
Zaremba SK (1966) Good lattice points, discrepancy, and numerical integration. Ann Mat Pur Appl 293:4–73